Numerical Simulation of the Aeroacoustic Noise in the Separated Laminar Boundary Layer

Hyo Won Choi, Young J. Moon*, Kyu-Jung Lee
Department of Mechanical Engineering, Korea University, Seoul 136-701, Korea

The unsteady flow characteristics and the related noise of separated incompressible laminar boundary layer flows (Re_{δ^*}=614, 868, and 1,063) are numerically investigated. The characteristic lines of the wall pressure are examined to identify the primary noise source, related with the unsteady motion of the vortex at the reattachment point of the separation bubble. The generation and propagation of the vortex-induced noise in the separated laminar boundary layer are computed by the method of Computational Aero-Acoustics (CAA), and the effects of Reynolds number, Mach number and adverse pressure gradient strength are examined.

Key Words : Unsteady, Laminar, Separation Bubble, Vortex Shedding, Aero-Acoustic Noise

1. Introduction

The separated laminar boundary layer flows are often encountered around airfoils under the influence of local adverse pressure gradient. For example, at incidences below the stall, a transition occurs due to the unsteady leading edge separation bubble on the airfoil. A typical structure of the time-mean laminar boundary layer separation bubble is described by Horton(1968), as shown in Fig. 1.

The unsteady feature of the separation bubble is distinguished as: (i) separation build-up and (ii) periodic shedding of the cross-stream vortices. The strong vortex generation and shedding in the separation bubble was visualized by Koromilas and Telionis(1980). Kloker and Fasel (1993) and Zhang et al. (2000) [Bestek et al. (1989)] also showed that the behavior of the separation bubble becomes unsteady and this unsteadiness is attributed to the transition of the separated laminar boundary layer. Pauley et al. (1990) also numerically investigated the critical condition of the periodic vortex shedding in the unsteady laminar boundary layer separation and found an invariant property of Strouhal number regardless of Reynolds numbers and suction strengths.

In the present study, our attention is focused on understanding the unsteady motion of the vortex near the reattachment point of the separation bubble, since its interactions with the adjacent wall possibly become an aero-acoustic noise source. A computational aero-acoustic (CAA) method (Shen and Sorensen, 1999) is used to simulate the generation and propagation of the acoustic noise in the separated laminar boundary layer, with the acoustic sources appropriated from

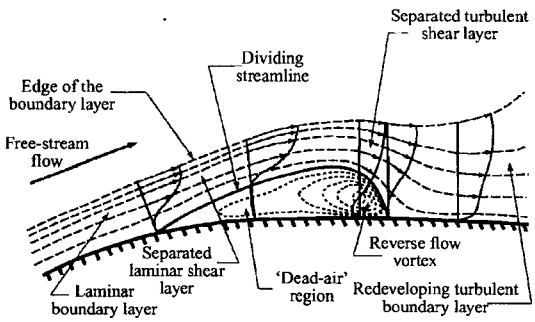

Fig. 1 A time-mean flow structure of laminar separation bubble (Horton, 1968)

* Corresponding Author,
E-mail : yjmoon@korea.ac.kr
TEL : +82-2-3290-3358; **FAX** : +82-2-926-9290
Department of Mechanical Engineering, Korea University, 1-5 Anam-dong, Sungbuk-ku, Seoul 136-701, Korea. (Manuscript **Received** February 18, 2002; **Revised** November 5, 2002)

the computational fluid dynamics (CFD) calculations.

2. Computational Methodology

There exits a large disparity between the aerodynamic scales and the acoustic ones, if the flow Mach number is close to an incompressible flow limit. For this reason, a splitting method proposed by Hardin and Pope (1994) and Shen and Sorensen (1999) is employed, which decouples the direct numerical simulation (DNS) approach into an incompressible flow problem and an acoustically perturbed one. In the present study, the incompressible Navier-Stokes equations are time-accurately solved by a projection method based algorithm. Then, the time-periodic viscous flow solutions are coupled into the acoustic field computation, solving for a set of acoustically perturbed Euler equations with the structured cartesian mesh.

2.1 Incompressible flow solver algorithms

The incompressible Navier-Stokes equation is time accurately solved by a projection method based algorithm (Hirt and Cook, 1972).

$$\frac{\partial u_i}{\partial x_i}=0 \tag{1a}$$

$$\frac{\partial u_i}{\partial t}+\frac{\partial u_i u_j}{\partial x_j}=-\frac{\partial p}{\partial x_i}+\frac{1}{Re}\frac{\partial}{\partial x_j}\left(\frac{\partial u_i}{\partial x_j}\right) \tag{1b}$$

The governing Eq. (1) is spatially discretized by a cell-center based finite-volume method. A second-order upwind differencing scheme is used for the convective flux terms, while the terms related to the viscous fluxes are treated by a centered scheme. The Poisson equation is then implicitly solved by an alternate directional implicit (ADI) method with a double sweep. Numerical details of the solution method are described in the reference [Moon and Koh(2001)].

2.2 Computational aero-acoustic algorithms

The acoustic fields are computed by a splitting method proposed by Shen and Sorensen (1999). The instantaneous velocities, pressure, and density are decomposed into the hydrodynamic variables and the acoustically perturbed quantities denoted by a prime,

$$\begin{aligned} u_i(x,\ t)&=U_i(x,\ t)+u_i'(x,\ t)\\ p(x,\ t)&=P(x,\ t)+p'(x,\ t)\\ \rho(x,\ t)&=\rho_0+\rho'(x,\ t)\end{aligned} \tag{2}$$

Inserting the decomposed variables into the compressible Navier-Stokes equations, a set of acoustic field equations are derived by subtracting the incompressible Navier-Stokes equations from them:

$$\frac{\partial \rho'}{\partial t}+\frac{\partial f_i}{\partial x_i}=0 \tag{3}$$

$$\frac{\partial f_i}{\partial t}+\frac{\partial}{\partial x_j}[f_i(U_j+u_j')+\rho_0 U_i u_j'+p'\delta_{ij}]=0 \tag{4}$$

$$\frac{\partial p'}{\partial t}+c^2\frac{\partial f_i}{\partial x_i}=-\frac{\partial P}{\partial t} \tag{5}$$

where, $f_i=\rho u_i'+\rho' U_i$, $c^2=\gamma p/\rho$ and $\gamma=1.4$ is a ratio of specific heats.

Equations (2) ~ (5) are numerically solved by the second-order accurate MacCormack's predictor-corrector scheme, in coupled with the unsteady incompressible flow computations. For the present scheme, 20~25 mesh points are used per one acoustic wavelength, which is strictly required in order to properly resolve the wave propagation with the least numerical diffusion and dispersion errors(Hardin and Pope, 1994). In the computation, a fourth-order artificial dissipation term is also added to Eqs. (3) ~ (5) to stabilize the numerical scheme.

In computational acoustics, the problems involving wave reflections are issued very importantly because the physical domains are necessarily truncated due to the limitation of the finite computational domain. Thus, at these artificial boundaries, non-reflecting or absorbing numerical boundary conditions are needed so that outgoing waves are not reflected into the computational domain. In the far-field buffer zones, the Perfectly-Matched Layer (PML) equations(Hu, 1996) are applied by splitting each of the flow variables ($\rho'=\rho_1'+\rho_2'$) and segregating the spatial gradients into each split equation (the ρ_1' equation only includes the x_1-gradients).

3. Computational Results and Discussion

3.1 Periodic vortex shedding in the laminar separation bubble

In order to understand the nature of aero-acoustic noise generation from an unsteady laminar separation bubble, the work of Henk (1990) and Pauley et al. (1990) is re-considered. As shown in Fig. 2, a laminar boundary layer with the zero pressure gradient is exposed to a sudden local adverse pressure gradient by initiating the suction through a port on the control wall (upper wall). With the suction strength above the critical condition, the laminar boundary layer separates and periodic vortex sheddings occur in the bubble. In the present study, the same computational mesh systems and boundary conditions as in Pauley et al. (1990) were used.

For investigating the unsteady flow characteristics of the separation bubble, parametric studies have been conducted for the cases of flow conditions summarized in Table 1. Here, a local Reynolds number, Re_x, is defined by the length measured from the channel entrance to the suction port (beginning point) and the free-stream velocity. Also, S, defined as a fraction of the entering flow removed through the suction port, controls the strength of adverse pressure gradient imposed on the boundary layer. The cases considered in Table 1 correspond to Re_{δ^*}=614, 868, and 1063 in terms of the Reynolds number based on boundary layer displacement thickness, and all are within the laminar shear layer instability, i.e., $600<Re_{\delta_*}<3000$. The periodic vortex shedding in the separation bubble is caused by a feedback mechanism between the laminar shear layer instability and the upstream propagating pressure waves generated at the vortex break-up stage.

Table 1 Flow conditions

Re_x	1.2×10^5			2.4×10^5			3.6×10^5		
M_∞	0.1			0.2			0.3		
δ/H	0.0687			0.0486			0.0397		
Re_{δ^*}	614			868			1,063		
S	0.22	0.27	0.32	0.22	0.27	0.32	0.22	0.27	0.32

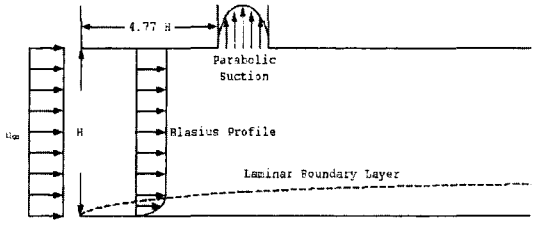

Fig. 2 Hydrodynamic computational domain

The unsteady laminar separation bubble can be characterized by the four-stage motions of the shed vortex in a period : (a) roll-up, (b) break-up, (c) rolling, and (d) ejection. Figure 3 shows

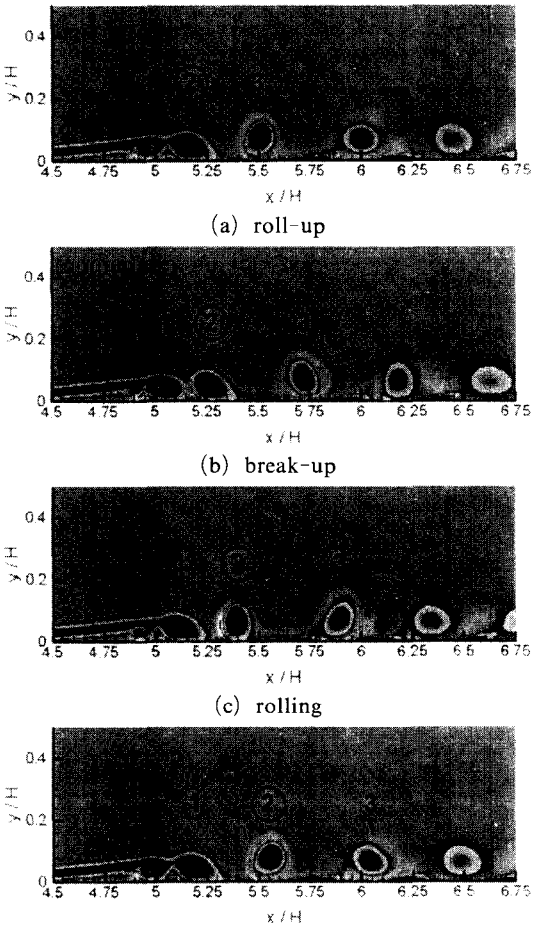

(a) roll-up

(b) break-up

(c) rolling

(d) ejection

Fig. 3 Instantaneous vorticity contours at four stages in a period ($Re_x=3.6\times10^5$, $S=0.22$) : base on ②

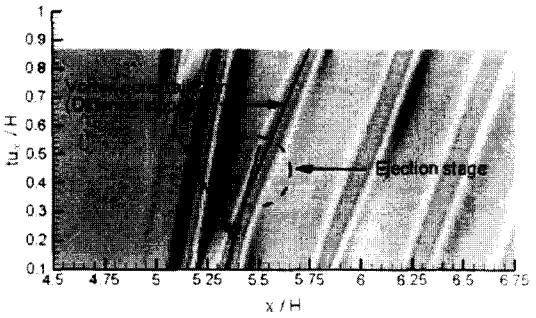

Fig. 4 Wall pressure characteristic lines (Re_x=3.6×10^5, S=0.22)

those four-stage motions (based on vortex ②), in terms of the instantaneous vorticity contours (Re_x=3.6×10^5 and S=0.22). First of all, it is of our interest to identify which vortical motion among four plays a dominant role as a noise source in the separation bubble. Hereby, the characteristic lines of the wall pressure are examined in Fig. 4, which represent the trajectories and speeds of the shed vortices in the separation bubble and downstream. One can clearly notice a slope difference between the characteristic lines at the ejection stage. The ejection stage is the one at which a shed vortex (e.g. ②) is ejected from the wall, with rapid change of rotational and convectional speeds. This simply causes the wall pressure to fluctuate and is conjectured as an aero-acoustic noise source.

Second of all, it is interesting to examine whether the vortex ejection location is an invariant property regardless of Reynolds numbers and suction strengths, for which the vortex shedding frequency St_θ=0.00686±0.6% is true, found by Pauley et al. (1990). Here St_θ is based on the boundary layer momentum thickness (θ) at the separation point and the local free-stream velocity. In the present study, the vortex ejection location, E, is defined as a distance between the ejection location and the reattachment point of the bubble (in a time-averaged sense), which are then normalized by the separation bubble size, i.e., $E=(x_E-x_R)/L_B$. Here, x_E, x_R, and L_B are the vortex core position at the ejection, the reattachment point, and the separation bubble size, respectively. The time-mean flow structure

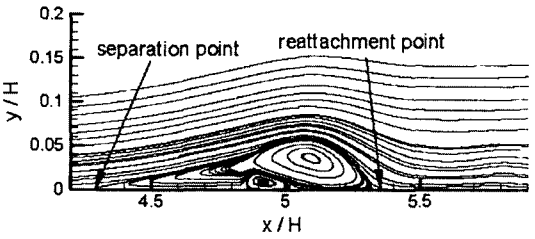

(a) A time-mean flow structure (Re_x=3.6×10^5, S=0.22)

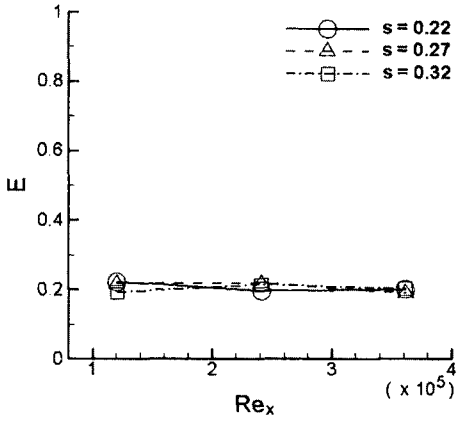

(b) Normalized vortex ejection location

Fig. 5 Time-mean flow characteristics of the separation bubble

of the separation bubble was obtained by using a time interval of twenty periods. Figure 5(a) shows the time-averaged streamlines of the separation bubble (Re_x=3.6×10^5 and S=0.22), from which one can clearly define the separation/reattachment points and the bubble size. In Fig. 5 (b), the normalized relative vortex ejection location is plotted for all test cases summarized in Table 1. The figure shows that E collapses to 0.2±1% for all cases, indicating that E is an invariant property regardless of Reynolds numbers and suction strengths.

3.2 Aeroacoustic noise generation

The aeroacoustic noise generated by periodic vortex sheddings in the separated laminar boundary layer is computed on the cartesian meshes by the CAA method described in Section 2.2. The acoustic computational domain is determined with considerations as follows. For the case of flow Mach number 0.3, the computed Strouhal

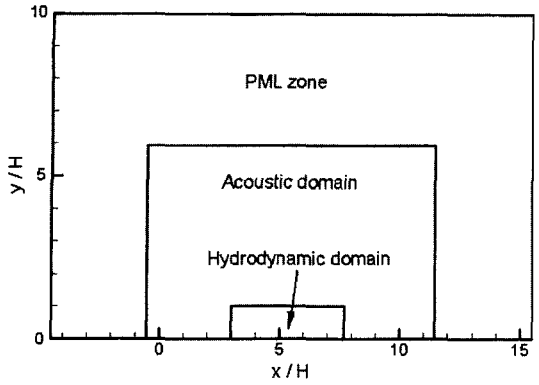

Fig. 6 Acoustic computational domain

Table 2 Absorption parameters for PML B.C.

Re_x	M_∞	S	λ/H	Absorption function	D	σ_m	β
1.2×10^5	0.1	0.22	15.9	Type A	6	100	1.5
		0.27	15.3				
		0.32	14.9				
2.4×10^5	0.2	0.22	5.4	Type B	18	17	2.0
		0.27	5.25				
		0.32	5.15		4		
3.6×10^5	0.3	0.22	2.9			5	
		0.27	2.87				
		0.32	2.83				

Type A : $\sigma=\sigma_m(\tanh(\beta(x-0.35D))+\tanh(0.5\,D\beta))$

Type B : $\sigma=\sigma_m(d/D)^\beta$

number of the flow oscillation based on the channel height is 1.15 and the acoustic wavelength of the radiated sound wave can be estimated as approximately 2.9 according to the relation $\lambda/H=1/(St_H\cdot M_\infty)$. Therefore the acoustic computational domain, as shown in Fig. 6, is set from $-4.5H$ to $15.5H$ in the x-direction and from 0 to $10H$ in the y-direction in order to include 2 or 3 wavelengths of the sound wave and to cover at least more than 1 wavelength in the PML zone.

In the present study, our attention is focused on noise generated by unsteady vortex motions near the boundary layer separation bubble. Therefore the noise sources are confined to the region, $x_S-0.3L_B<x<x_R+0.3L_B$ and $0<y<5\delta$ for all cases. Here x_S and δ denote the separation point and the boundary layer thickness. The uniform cartesian meshes of 501×251 are used for the acoustic field computation, in order to keep the proper resolution of the vortex motions in the separated boundary layer. This automatically fulfills the requirement such that 20~25 points be included per wavelength in order to minimize the numerical dispersion and dissipation errors of the MacCormack's second-order scheme (Hardin and Pope, 1994).

The proper selection of PML zone thickness is computationally very important in order to effectively damp out the out-going waves through the boundaries. Table 2 summarizes the absorption parameters used in the PML zone for the cases considered. Here λ/H, D, d, σ_m, and β are the normalized wavelength, PML zone thickness, distance from the interface with the interior domain, and absorption coefficient, respectively. For the low Mach number case ($M_\infty=0.1$), a considerably higher damping coefficient (σ_m) is used with the damping function of type A, in order to introduce a thicker damping level in the PML zone for the long wave ($\lambda/H=15$).

The instantaneous acoustic pressure field contours shown in Fig. 7(a) well visualize the main tonal sound wave generation from an unsteady separation bubble for $Re_x=3.6\times10^5$, $M_\infty=0.3$, and $S=0.22$. It is also interesting to note that the short waves are constantly generated between the main tonal waves. By closely examining the acoustic fields near the reattachment point of the separation bubble, the main tonal wave is generated by the vortex ejection motion adjacent to the wall; it causes the wall pressure to drop suddenly, creating a local expansion, while, right after the ejection, the pressure field is immediately recovered with a local compression back. The computed wavelength of the main tonal sound is approximately 3, which is quite close to the estimated value of 2.9 by the relation, $\lambda/H=1/(St_H\cdot M_\infty)$. The short waves are also generated when the vortex is at roll-up, break-up, and rolling, but the detail of generation mechanism needs to be studied.

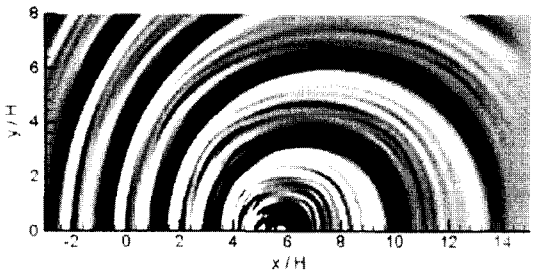

(a) Instantaneous acoustic pressure field

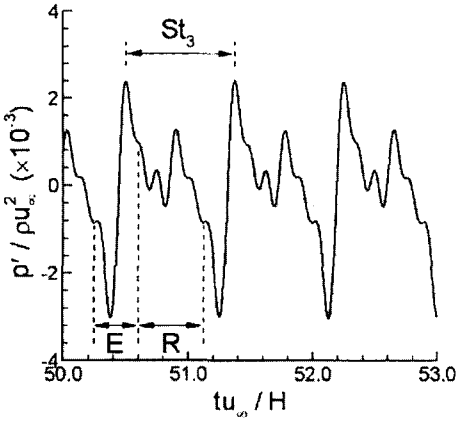

(b) Acoustic pressure variation (E : ejection, R : the rest)

Fig. 7 Acoustic pressure waves from the separation bubble ($Re_x=3.6\times10^5$, $M_\infty=0.3$, $S=0.22$)

In the present study, a reference observer's position is set on the point five times the separation bubble size away from the reattachment point in the direction of 135°, since the noise sources are near the reattachment point of the bubble and the highest intensity of the radiated sound noise is approximately between 90°~180°. Figure 7(b) shows the acoustic pressure variations in time at the reference point. It clearly indicates that the main tonal sound pressure variations occur during the time period of vortex ejection motion (indicated by E in the figure). Here St_3 indicates the period corresponding to the non-dimensional frequency, Strouhal number of the present $M=0.3$ case, and St1 and St_2 in Fig. 10 and 11 represent also the Strouhal numbers of $M=0.1$ and 0.2 cases.

As shown before, an acoustic wavelength can be calculated by a relation $\lambda/H=1/(St_H\cdot M_\infty)$. This relation can be rewritten as $\lambda=(U_\infty/f)/M_\infty$,

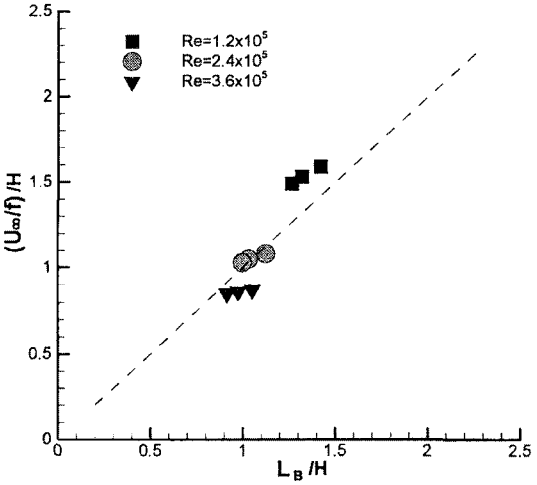

Fig. 8 A correlation between the characteristic eddy size ($\equiv U_\infty/f$) and the separation bubble size (L_B)

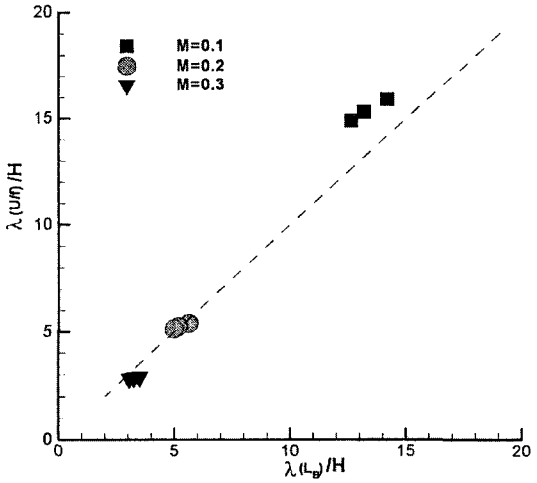

Fig. 9 A correlation between the acoustic wavelengths based on two length scales (U_∞/f and L_B)

where U_∞/f can be regarded as a characteristic eddy size of the separation bubble. It is shown in Fig. 8 that U_∞/f is reasonably well correlated to the separation bubble size (L_B) (time-averaged). This means that the acoustic wavelength can also be expressed as $\lambda\approx L_B/M_\infty$. The acoustic wavelength obtained by this relationship is correlated to $\lambda=(U_\infty/f)/M_\infty$ in Fig. 9.

In Fig. 10, the acoustic pressures are also compared for three different Reynolds numbers of

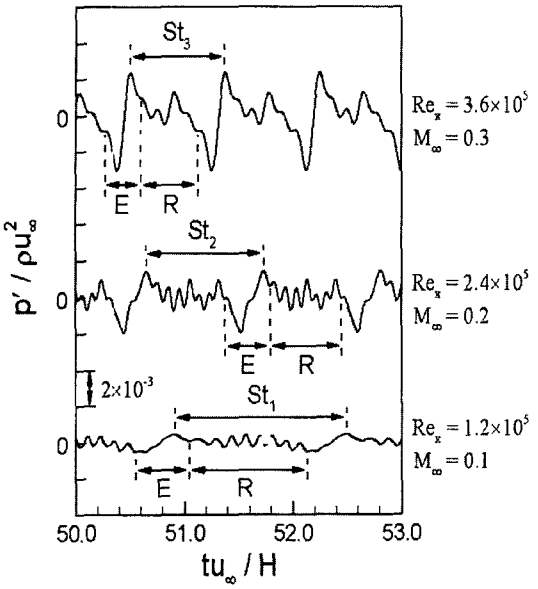

Fig. 10 Acoustic pressures for various Re_x (or M_∞) (S=0.22)

Re_x=3.6×10^5, Re_x=2.4×10^5, and Re_x=1.2×10^5 with corresponding Mach numbers of 0.3, 0.2, and 0.1. For all cases, the acoustic pressure variations in 'E' are identified as the main tonal sound wave. One can also notice that the acoustic pressure level and frequency increase, as the Reynolds number (or Mach number) increases. The frequency increase is due to the local Reynolds number effect, because the Reynolds number directly determines the length scale of the boundary layer at separation and therefore the vortex shedding frequency. The acoustic pressure level dependence is, however, not quite clear, since the strength of the shed vortex in the bubble also depends on the Reynolds number.

Therefore, the acoustic pressure has been tested for the following conditions: (i) with the same Reynolds number of Re_x=3.6×10^5 and suction strength of S=0.22 but different Mach numbers of 0.1 and 0.3, (ii) with the same Mach number of 0.1 and suction strength of S=0.22 but the different Reynolds numbers of Re_x=1.2×10^5 and Re_x=3.6×10^5, and (iii) with the same Mach number of 0.3 and Reynolds number of Re_x= 3.6×10^5 but different suction strengths of S=0.22 and S=0.32. Figure 11 shows (a) the Mach num-

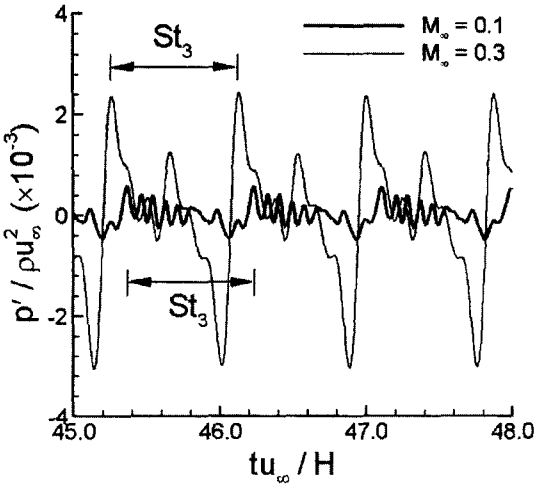

(a) Mach number effect (Re_x=3.6×10^5, S=0.22)

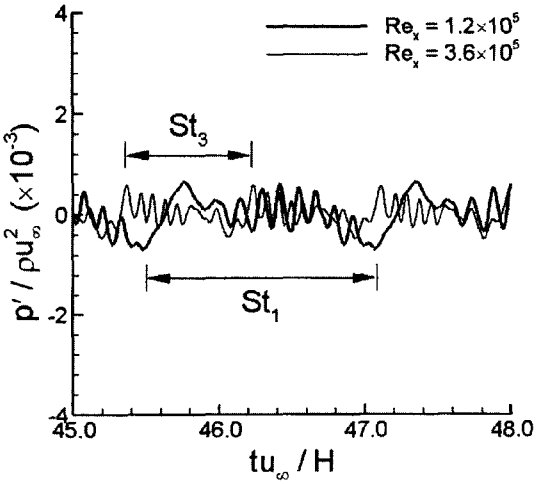

(b) Reynolds number effect (M_∞=0.1, S=0.22)

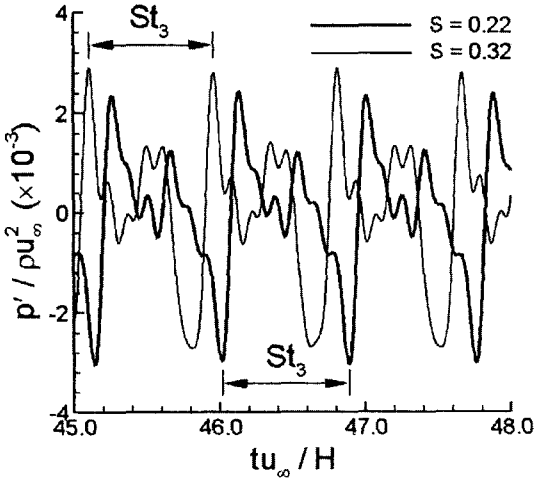

(c) Suction strength effect (M_∞=0.3, Re_x=3.6×10^5)

Fig. 11 Acoustic pressure comparison

ber effect, (b) the Reynolds number effect, and (c) the suction strength effect on the acoustic pressure variations during the four-stage motions of the shed vortex in the separation bubble. It is indicated that, although the frequency is affected by the local Reynolds number, the acoustic pressure level is primarily affected by the Mach number of the flow. It is also indicated that the suction strength has little influence on the frequency nor the acoustic pressure variations.

4. Conclusion

The unsteady flow characteristics and the related noise of separated incompressible laminar boundary layer flows are numerically investigated. It is shown that the periodic vortex shedding in the separation bubble is composed of four-stage unsteady vortex motions: roll-up, break-up, rolling, and ejection, and the ejection motion is conjectured as a primary noise source in the separation bubble. It is also interesting to note that, for all flow conditions, the vortex ejection location relative to the reattachment point is $0.2 \pm 1\%$ (normalized by the bubble size), which is an invariant property regardless of Reynolds numbers and suction strengths.

The acoustic pressure contours showed a main tonal sound wave generated from the separation bubble, accompanied by the short waves. Among the four stage vortex motions, the vortex ejection is identified as a main noise source, and the acoustic pressure levels are primarily affected by the flow Mach number, in comparison with the Reynolds number and suction strength.

Acknowledgment

This work was supported by a Korea University Grant for the year of 2001.

References

Hardin, J. C. and Pope, D. S., 1994, "An Acoustic/Viscous Splitting Technique for Computational Aeroacoustics," *Theoretical and Computational Fluid Dynamics*, Vol. 6, No. 5-6, pp. 323~340.

Henk, R. W., 1990, "An Experimental Study of the Fluid Mechanics of an Unsteady, Three-dimensional Separation," Ph. D. Thesis, Stanford University.

Hirt, C. W. and Cook, J. L., 1972, "Calculating Three-Dimensional Flows Around Structures and over Rough Terrain," *Journal of Computational Physics*, Vol. 10, pp. 324~340.

Horton, H. P., 1968, "Laminar Separation Bubbles in Two-and Three-Dimensional Incompressible Flow," Ph. D. Thesis, University of London.

Hu, F. Q., 1996, "On Absorbing Boundary Conditions for Linearized Euler Equations by a Perfectly Matched Layer," *Journal of Computational Physics*, Vol. 129, pp. 201~219.

Kloker, M. and Fasel, H. F., 1993, "Direct Numerical Simulations of Boundary Layer Transition under Strong Adverse Pressure Gradient," *Proc. IUTAM Symp. Laminar-Turbulent Transition*, Sendai, Japan.

Koromilas, C. A. and Telionis, D. P., 1980, "Unsteady Laminar Separation : an Experimental Study," *Journal of Fluid Mechanics*, Vol. 97, pp. 347~384.

Moon, Y. J. and Koh, S. R., 2001, "Counter-Rotating Streamwise Vortex Formation in the Turbine Cascade with Endwall Fence," *Computers & Fluids*, Vol. 30, pp. 473~490.

Pauley, L. L., Moin, P. and Reynolds, W. C., 1990, "The Structure of Two-Dimensional Separation," *Journal of Fluid Mechanics*, Vol. 220, pp. 397~411.

Shen, W. Z. and Sorensen, J. N., 1999, "Comment on the Aeroacoustic Formulation of Hardin and Pope," *AIAA Journal*, Vol. 37, No. 1, pp. 141~143.

Zhang, H. L., Bachman, C. R. and Fasel, H. F., 2000, "Reynolds-Averaged Navier-Stokes Calculations of Unsteady Turbulent Flow," *AIAA Paper* 2000-0143.